

1 **Capturing the diversity of mesoscale trade wind cumuli**  
2 **using complementary approaches from self-supervised**  
3 **deep learning**

4 **Dwaipayan Chatterjee<sup>1</sup>, Sabrina Schnitt<sup>1</sup>, Paula Bigalke<sup>1</sup>, Claudia**  
5 **Acquistapace<sup>1</sup>, Susanne Crewell<sup>1</sup>**

6 <sup>1</sup>Institute for Geophysics and Meteorology, University of Cologne, Cologne, Germany

7 **Key Points:**

- 8 • Mesoscale cloud organization can be taxonomized by a two-step deep learning ap-  
9 proach in the feature space continuum  
10 • Comparing seven machine-identified classes with humans' four recognized cate-  
11 gories underlines the significance of uncertainty estimates  
12 • New diagnostic is provided to analyze the temporal transition between regimes,  
13 as illustrated for human-labeled sugar-to-flower regimes

---

Corresponding author: Dwaipayan Chatterjee, [dchatter@uni-koeln.de](mailto:dchatter@uni-koeln.de)

## 14 Abstract

15 At mesoscale, trade wind clouds organize with various spatial arrangements, shaping  
 16 their effect on Earth’s energy budget. Representing their fine-scale dynamics even  
 17 at 1 km scale climate simulations remains challenging. However, geostationary satellites  
 18 (GS) offer high-resolution cloud observation for gaining insights into trade wind cumuli  
 19 from long-term records. To capture the observed organizational variability, this work pro-  
 20 poses an integrated framework using a continuous followed by discrete self-supervised  
 21 deep learning approach, which exploits cloud optical depth from GS measurements. We  
 22 aim to simplify the entire mesoscale cloud spectrum by reducing the image complexity  
 23 in the feature space and meaningfully partitioning it into seven classes whose connec-  
 24 tion to environmental conditions is illustrated with reanalysis data. Our framework fa-  
 25 cilitates comparing human-labeled mesoscale classes with machine-identified ones, ad-  
 26 dressing uncertainties in both methods. We highlight the potential to explore transitions  
 27 between regimes, a challenge for physical simulations, and illustrate a case study of sugar-  
 28 to-flower transitions.

## 29 Plain Language Summary

30 Clouds are a fundamental player affecting our planet’s energy balance, making their  
 31 accurate representation crucial in climate models. One open question is how they orga-  
 32 nize on a scale of a few 100 km (mesoscale) in the tropical northern Atlantic region east  
 33 of Barbados. Satellite observations can help to categorize these clouds, but previous meth-  
 34 ods had limitations in capturing the full range of cloud arrangements and transitions be-  
 35 tween different cloud forms. We have introduced a novel approach that utilizes machine  
 36 learning and geostationary satellite data to address this issue. Our machine learning model  
 37 autonomously learns to recognize various cloud patterns and distributions. We conducted  
 38 a comparative analysis between the categories generated by the machine and those iden-  
 39 tified by human experts to understand the strengths and weaknesses of both methods.  
 40 Additionally, we explore a case study where clouds undergo a transformation, changing  
 41 from a structure resembling sugar to one resembling flowers. This particular transfor-  
 42 mation was found difficult to capture with physical simulation before. The clear signa-  
 43 tures of the transition identified by our machine learning approach can help to better  
 44 understand cloud evolution, which is crucial for improving climate models and predict-  
 45 ing how cloud behavior may change in a changing climate.

## 46 1 Introduction

47 Shallow convective clouds, though individually small (measuring in tens of meters),  
 48 cover large areas of the tropical oceans, forming distinct cloud fields that span hundreds  
 49 of km. They are vital in regulating the Earth’s energy balance, exerting a net cooling  
 50 effect by reflecting more sunlight than retaining outgoing long-wave radiation (Bony et  
 51 al., 2004). However, the representation of these clouds, even in the advanced 1km scale  
 52 climate simulations, is insufficient (Schneider et al., 2019). This contributes to a signif-  
 53 icant inter-model spread in predicted cloud feedback and climate sensitivity (Bony & Dufresne,  
 54 2005; Nuijens & Siebesma, 2019). To address this challenge, Bony et al. (2017) proposed  
 55 the EUREC<sup>4</sup>A field campaign, organized in January-February 2020, around the Barba-  
 56 dos region of the North Atlantic Trades (NAT) (Stevens et al., 2021). This initiative aimed  
 57 to enhance our understanding of shallow cloud dynamics by leveraging a diverse set of  
 58 observations and thus possibly improving their representation in numerical models.

59 During the preparation of the campaign Stevens et al. (2020) identified four shal-  
 60 low convective organization regimes (*Sugar, Gravel, Flower, Fish*) (SGFF), with frequent  
 61 occurrence on meso- $\beta$  (20 to 200 km) and meso- $\alpha$  (200 to 2,000 km) spatial scale. These  
 62 regimes exhibit differences in net cloud radiative feedback (Bony et al., 2020) and are

63 related to different environmental conditions (Schulz et al., 2021). Of specific interest  
 64 are transitions between different organizations, e.g., from sugar to flower, which has been  
 65 studied in Large-Eddy-Simulation (LES) to understand the governing processes and prove  
 66 to be difficult (Narenpitak et al., 2021; Dauhut et al., 2023).

67 Yet, imposing four distinct classes on the diversity of the observed organization does  
 68 not cover the intermediate cloud patterns or transient states, as highlighted by LES stud-  
 69 ies. Hence, some processes critical for climate feedback may be ignored or neglected. Fur-  
 70 thermore, recent studies trying to quantify these labeled well-organized systems find that  
 71 they occur only around 50% over NAT (Janssens et al., 2021; Schulz et al., 2021; Vial  
 72 et al., 2021) and some ambiguities in agreement from the labeler’s side exist (Schulz, 2022).

73 Denby (2020) and Janssens et al. (2021) argue for a continuum of cloud organiza-  
 74 tion where Denby (2020) employs an unsupervised neural network for grouping similar  
 75 cloud structures and demonstrate its effectiveness via hierarchical clustering (HC) and  
 76 associated radiative properties. However, their training approach involved biased, false  
 77 negative sampling (Huynh et al., 2022). Further, employing high-dimensional features  
 78 in HC has performance and scalability issues (Du, 2023; Gilpin et al., 2013). Janssens  
 79 et al. (2021) assumes a linear combination of traditional cloud metrics for describing the  
 80 cloud systems. Utilizing these metric scores and a k-means algorithm, they attempted  
 81 to partition their metric space into seven arbitrary clusters, as finding the optimal clus-  
 82 ters seemed non-trivial.

83 The overarching goal of our study is to develop a simplified approach to describe  
 84 cloud organization from high-resolution images. In this way, it should open up new path-  
 85 ways to exploit the information content of existing comprehensive satellite data records.  
 86 Our first objective is to develop a simplified, streamlined representation that captures  
 87 the entire cloud spectrum’s organizational relationships, which we call a continuum. Sec-  
 88 ond, we target the four somewhat arbitrary classes from Stevens et al. (2020) and delve  
 89 deeper into finding the optimal partitions of a meaningful and interpretable continuum.  
 90 We approach our objectives by developing a two-step self-supervised deep learning ap-  
 91 proach (Section 3) applied on GOES – 16 E cloud optical depth (COD) images (Section  
 92 2). Section 4.1 delves deeper into the representations and their characteristics, highlight-  
 93 ing the differences to Denby (2023)’s approach. Our work demonstrates that the pres-  
 94 ence of derived partitions facilitates a comparison of human labels with these partitions  
 95 (Section 4.2). Finally, in Section 5, we illustrate how the partitioning of the continuum  
 96 supported by environmental data allows us to monitor when a particular cloud system  
 97 transitions to another.

## 98 **2 Satellite dataset**

99 We use COD retrieved from GOES-16 E Advanced Baseline Imager (Schmit et al.,  
 100 2005) using the daytime cloud optical and microphysical properties algorithm (DCOMP)  
 101 (Walther & Heidinger, 2012) at 2 km horizontal resolution and 10 – 15 minutes tempo-  
 102 ral resolution. Our domain in NAT (5 – 20° N and 40 – 60° W) is similar to domains used  
 103 in past studies (Bony et al., 2020; Schulz et al., 2021). The regional climate defines De-  
 104 cember to May as dry and June to November as wet seasons (Stevens et al., 2016). We  
 105 consider November to April 2017 - 2021 as our study period. November is added to the  
 106 typical dry period because we want to see how stronger convective events influence our  
 107 approach.

108 We chose COD because it is closely related to the cloud radiative effect and mit-  
 109 igates solar and surface influences. The uncertainty associated with COD retrieval re-  
 110 mains below 10% for all ranges in water clouds (see Figure 4 in Walther and Heidinger  
 111 (2012)). Note that some fine-scale cloud systems, such as sugar and gravel (meso- $\beta$  scale),  
 112 their individual cloud cells might not be fully resolved with the spatial resolution of this

113 product. However, since our study focuses on the organizational aspects of shallow con-  
 114 vection clouds (spanning hundreds of km), we expect the resolution limit to have a lim-  
 115 ited impact on our study.

116 Representation learning, also known as feature learning, is a specialized field within  
 117 machine learning that focuses on extracting meaningful features of a given dataset. To  
 118 better represent the mesoscale cloud distributions, we use six images per timestamp, in-  
 119 cluding an additional fixed image over the Barbados domain (see S1). Although they might  
 120 overlap in some instances, random cropping aims to get mesoscale distributions as di-  
 121 verse as possible without human interference. Note that the Barbados domain enables  
 122 comparison with ground-based measurements in future studies. To have an adequate spa-  
 123 tial scale of typical occurring cloud fields over NAT (as discussed in Section 1), we use  
 124 256 x 256 pixels (roughly 512 square km) as also found in Muller and Held (2012). We  
 125 exclude crops affected by glint or poor retrieval quality using the respective data flags.  
 126 Time stamps are limited to 9 am - 3 pm Barbados local time to avoid sun glinting. We  
 127 use land class data to filter out images with convection over land, specifically over the  
 128 northeast of the South American continent. Finally, to mitigate uncertainties at high COD  
 129 from DCOMP retrieval, COD values above a threshold of 50, already indicating deep clouds,  
 130 are clipped to 50. This results in a sample size of 51,000 satellite images.

131 For further analysis, we make use of hourly ERA-5 (Hersbach et al., 2020) large-  
 132 scale environmental parameters (integrated water vapor (IWV), horizontal and vertical  
 133 wind speed, relative humidity) and cloud fraction at a spatial resolution of 0.25°. Hourly  
 134 cloud amount for four vertical ranges (surface-700 hPa, 700 hPa-500 hPa, 500 hPa-300  
 135 hPa, 300 hPa-tropopause) is used from the Clouds and Earth’s Radiant Energy System  
 136 fourth edition (CERES, Edition - 4A) (Wielicki et al., 1996), characterized by a spatial  
 137 resolution of 1°.

### 138 3 Methods

139 The workflow is as follows: a) A neural network (N1) ingests satellite images to con-  
 140 tinuously sort cloud organizations based on visual similarity, yielding the feature vec-  
 141 tor 'Z' (384 dimensions) for each image. b) Z is reduced to a 2-dimensional (2D) space  
 142 for visualizing a continuous arrangement of images with respect to their cloud structures  
 143 (continuum). c) The optimal number of clusters is derived from the 2D representation  
 144 (t-SNE), d) A second neural network (N2) of similar architecture as N1 but constrained  
 145 by 'K' classes ingests the satellite images to finally assign each image to a discrete class.

146 a) We develop N1, whose purpose is to let the network identify the structural sim-  
 147 ilarities in the cloud systems and map the learned visual features into the 384-dimensional  
 148 feature space. We use the software package DINO from Facebook Artificial Intelligence  
 149 Research (FAIR) (Caron et al., 2021) based on PyTorch (Paszke et al., 2019) and the  
 150 open-source VISSL computer vision library (Goyal et al., 2021) to adapt the network to  
 151 our requirements. As a backbone neural architecture to process images, we use Vision  
 152 Transformer (ViT), which has a sequence of self-attention (Vaswani et al., 2023) and feed-  
 153 forward layers (Bebis & Georgiopoulos, 1994) paralleled with skip connections. This setup  
 154 helps to identify long-range spatial dependencies by learning relevant information in the  
 155 image (Khan et al., 2022). Eliminating the issue of false negative sampling from (Denby,  
 156 2020) but still focusing on learning similar embeddings of semantically similar mesoscale  
 157 distributions, every epoch, we opt for two random global crops with a 0.75 fraction (192  
 158 x 192 pixels) of the parent satellite image. As the largely overlapping global-crop pair  
 159 has very similar cloud structures, the network learns their essential features and puts the  
 160 pair closer to each other in the high-dimensional feature space. More details are given  
 161 in S2.

162 b) Z includes the continuously sorted representation of cloud organization. We re-  
 163 duce its 384-dimension dimensions to two dimensions using the well-established t-distributed  
 164 Stochastic Neighbor Embedding (t-SNE) algorithm (van der Maaten & Hinton, 2008).  
 165 t-SNE preserves relative local positions by using cosine distance in affinity computation  
 166 and tries to retain global structure by initializing with principal components for map-  
 167 ping to a two-dimensional space. This proves helpful because high-dimensional data when  
 168 directly applied to cluster analysis, face challenges like the curse of dimensionality (Aggarwal  
 169 et al., 2001), where increased dimensions make distances between data points less mean-  
 170 ingful. Also, the presence of noise and outliers can distort clusters, hindering the algo-  
 171 rithm’s ability to identify distinct clusters (Steinbach et al., 2004).

172 c) After obtaining the continuously sorted 2D representation of cloud systems (see  
 173 Fig. 1.a), we intend to find optimal boundary conditions within the sorted order to de-  
 174 rive distinct clusters (cloud regimes). Selecting a meaningful and interpretable number  
 175 of clusters is crucial to avoid over-fitting, where excessive clusters can capture noise, and  
 176 also under-fitting, where too few clusters can miss significant patterns in the data. On  
 177 this 2D representation space, we apply a set of three statistical approaches, namely met-  
 178 ric scores of distortion, silhouette (Rousseeuw, 1987), and Calinski-Harabasz (Caliński  
 179 & Harabasz, 1974) to identify the number of optimal classes into which the given fea-  
 180 tures could be clustered. Schubert (2023) suggests taking a collective inference from these  
 181 three methods to best fit the spherical k-means clustering algorithm used during the train-  
 182 ing of N2. S3 illustrates how the three metrics point to an optimal clustering into seven  
 183 classes. Note that the choice of seven classes is robust as illustrated by several sensitiv-  
 184 ity tests (shown in S4), such as the dimensionality-reduction technique, size of the dataset,  
 185 initial weights of the network, and different global crop sizes.

186 d) N2 from Chatterjee et al. (2023) learns to put each satellite image into one of  
 187 the seven classes as it progressively improves its feature space’s clustering, minimizing  
 188 the cross entropy between the two global random crops (192 x 192) from the parent satel-  
 189 lite image. Here, the main difference from N1 is that additional augmented image ver-  
 190 sions (random flipping and noise addition by random Gaussian blur) of global random  
 191 crops (see Fig. S2.2.b) are included. Augmentations try to provide auxiliary support to  
 192 the network’s generalizability and better capture the differences in diversity of the shal-  
 193 low cloud systems (Nie et al., 2021; Paletta et al., 2023). After obtaining the label of each  
 194 satellite image, we transfer the assigned class to the continuum space, which proves help-  
 195 ful because N1 has learned the sorting arrangement of keeping similar cloud systems closer.  
 196 Therefore, it helps to visualize how each cluster with distinct characteristics can form  
 197 a separate local region. Additionally, the N2 feature space is i) more sparse than N1 (see  
 198 S2 for explanation) and ii) arranged by closeness to the centroids, which, unlike N1, may  
 199 not be ideal for representing smooth transitions of cloud systems.

## 200 4 Results

### 201 4.1 Continuous and discrete representations

202 We now analyze the diversity of cloud systems included in the satellite data record  
 203 within their continuous and discrete representations. Both are visualized in 2D contin-  
 204 uum space using the t-SNE algorithm (Section 3). The organization state captured in  
 205 the satellite images changes smoothly and different cloud organizations can be identi-  
 206 fied in different areas of the continuum (Fig. 1.a). Going anticlockwise from the top, arch-  
 207 shaped cloud systems lie in the top-left, followed by flower-type distributions on the left  
 208 side of the continuum. Close to the flowers in the bottom-left are the flowers spreading  
 209 out into stratocumulus. Note that physically simulating the transition is challenging as  
 210 modeling studies struggle to capture the stratocumulus to cumulus transition (Sarkar  
 211 et al., 2020), although they lie adjacent in the continuum.

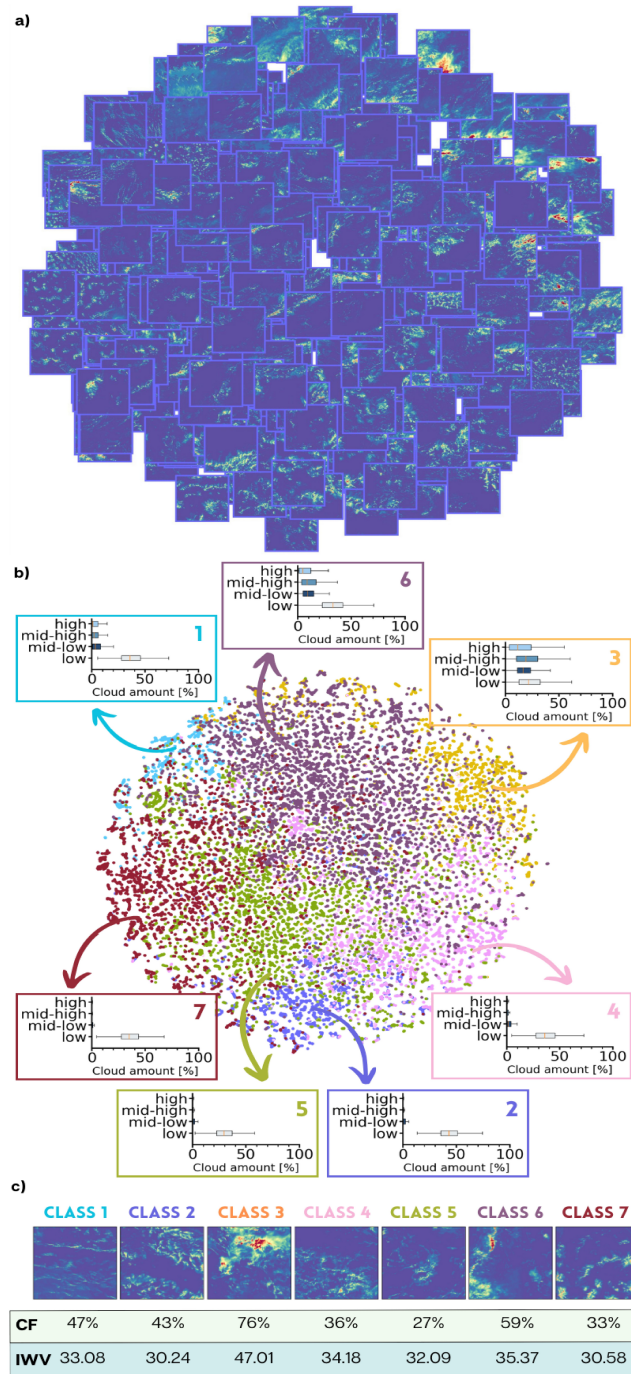


**Figure 1.** a) Visualization of four hundred randomly selected satellite images arranged in the continuum space. b) Same as a), but now, instead of an image, the discrete class determined by N2 is shown (colored). For each class, statistics on low, mid-low, mid-high, and high cloud amount (%) obtained from the CERES hourly data set are provided. c) Centroid COD images belonging to seven clusters as identified by the discrete neural network (N2). The table shows per class the average of cloud fraction (CF, %) from the GOES retrieval and integrated water vapor (IWV,  $\text{kgm}^{-2}$ ) from ERA-5.

212 The bottom part of the feature space contains long bony skeletons, i.e., fish-type  
 213 cloud systems, and the bottom-right corner shows an extended part of fish-type cloud  
 214 organizations delineated by unusually large cloud-free regions. The top-right region of  
 215 the continuum is a collection of deep convective cells. These primarily occur in the month  
 216 of November. Arc-shaped cloud systems appear on the left and top-left of the contin-  
 217 uum. Vogel et al. (2021) suggest that the horizontal structure of mesoscale arcs is in-  
 218 trinsically linked to gravel, flowers, and fish. In sequence, Figure 1a shows a continuous  
 219 link in the spatial arrangement of cloud systems rather than the distinct classes. This  
 220 demonstrates the good performance of our continuous approach, which is further sup-  
 221 ported by the analysis of attention maps in S5. Note that any newly taken satellite im-  
 222 age can be placed into this continuum using the weights of N1, allowing a quick assess-  
 223 ment of its organizational status. Also, similar trajectories of subsequent images can be  
 224 tracked within the continuum space.

225 After training N2, each of the images can be attributed to one of the seven classes  
 226 (refer to Section 3), revealing distinct spaces within the continuum (Fig. 1.b). To help  
 227 investigate how well the seven classes separate, they are evaluated using cloud amounts  
 228 at four different height levels from CERES data. This analysis, on the one hand, reflects  
 229 how each class differs from the others, and on the other hand, it reasons for the under-  
 230 lying closeness of each class with neighbor classes in the feature space. The difference  
 231 between the seven clusters is especially evident when looking at their centroid images  
 232 (Fig. 1.c).

233 Deep convective class three has by far the highest cloud fraction of 76% and a third  
 234 more water vapor ( $47.0 \text{ kgm}^{-2}$ ) than all other classes (mean =  $32.5 \text{ kgm}^{-2}$ ). We use IWV  
 235 as a fingerprint for the origin of air masses and intend to test it later to investigate the  
 236 connection between cloud regime and air mass origin. Figure 1.b already shows that class  
 237 3, which by far has the highest IWV, is also related to the deepest convection. Neigh-  
 238 boring class six includes less frequent higher-level clouds and has a reduced CF of 59%  
 239 compared to class three. All other classes are dominated by low-level clouds with lower  
 240 than 50% CF. Classes one and four (neighbor to class six) still have some mid to high-  
 241 level cloud amounts (below 10%). Class one can be interpreted as representing arch-shaped  
 242 cloud systems, and four resembles the fish class with a more open sky (also shown by  
 243 reduction in CF).

244 Classes two, five, and seven, being close in the continuum, have similar cloud ver-  
 245 tical distributions and IWV ranging from 30 to  $32 \text{ kgm}^{-2}$ ; however, their organization  
 246 is very different, as illustrated by the centroids (Fig. 1.c) and mean CFs (43%, 27%, and  
 247 33%, respectively). Class two primarily comprises shallow cloud cover, corresponding to  
 248 cloud systems resembling fish-type formations. Class five has the lowest cloud fraction  
 249 and is an intermediary class type between classes two and seven. Finally, class seven has  
 250 a presence of low cloud amounts and negligible mid to higher cloud amounts, which vi-  
 251 sually resembles flower-type cloud distributions. Therefore, discretizing the continuum  
 252 helps us visually find three main classes (one, two, and seven) frequently resembling fea-  
 253 tures identified by humans, i.e., sugar, fish, and flower, respectively. However, it also shows  
 254 the remaining diversity and their characteristics in a cohesive approach. Note that in con-  
 255 trast to the challenges faced by Denby (2023) or Janssens et al. (2021) in isolating mean-  
 256 ingful clusters, our N1 + N2 framework excels in efficiently categorizing the continuum  
 257 into seven interpretable classes. This intelligible partitioning not only simplifies cloud  
 258 organization complexities but also allows for the classification of unseen test data within  
 259 the continuum.

## 260 4.2 Machine versus human labels

261 While we checked for visual correspondence and class-wise characteristics in Sec-  
 262 tion 4.1, our framework now creates the opportunity to quantify how human labels com-

263 pare to the machine’s seven clusters. For this, we use the dataset from Schulz (2022),  
 264 which is a 1km x 1km resolution manually labeled dataset for the NAT region and EUREC<sup>4</sup>A  
 265 time period (47 days). Approximately 50 scientists generated the dataset by identify-  
 266 ing mesoscale patterns (SGFF) and marking variable-sized rectangles around homoge-  
 267 neous organization states. Overlapping rectangles allowed a single grid point to be la-  
 268 beled with multiple patterns by a scientist. Individual uncertainty is expressed through  
 269 each pattern’s classification mask ( $c_m$ ) (Schulz, 2022). For example, if a grid point is within  
 270 both gravel and sugar rectangles, the  $c_m$  would be 0.5 for both and 0 for the other two  
 271 patterns. Mutual agreement among scientists for each pattern at a grid point is deter-  
 272 mined by averaging  $c_m$  values, ranging from 0 to 100%.

273 We hypothesize patterns with higher agreement are most likely attributed to their  
 274 meaningful partitions within the continuum (as discussed in Section 4.1). For each time-  
 275 stamp where at least one of the four patterns was identified within our domain, we se-  
 276 lect a 256 x 256-pixel satellite image centered over the area of highest human agreement.  
 277 In this way, we ensure the best possible intercomparison. This leaves us with 52 sam-  
 278 ples of human-labeled satellite images (fish: 19.3%, gravel: 26.9%, flower: 28.8%, sugar:  
 279 25.0%). Note that even with the highest consensus criteria, there’s still diversity in agree-  
 280 ment. The inter-quartile agreement range is 35%, while the minimum and maximum agree-  
 281 ments show consensus levels of 7% and 91%, respectively.

282 The framework classifies 40% flower-labeled cloud systems in class seven (see the  
 283 hit rate for each class in Fig. 2.a) while sugar-labeled cloud systems are 31% classified  
 284 in class one and 20% in class four. Gravel has a total of 44% representation in classes  
 285 one and five, whereas fish annotated labels are allocated 30% in class two and 20% each  
 286 in classes four and five. Further, examining example images visually (Fig. 2.a), it be-  
 287 comes apparent that images with lower human agreement notably diverge from the es-  
 288 tablished definitions (provided in Stevens et al. (2020)) of SGFF cloud structures, in con-  
 289 trast to images with high human agreement.

290 Within the continuum (Fig. 2.b), flowers detected with high probability mostly oc-  
 291 cur in areas of class seven, which was already well reflected in the centroids. Following  
 292 a similar agreement is sugar (street-type cloud systems), which can be found in areas of  
 293 class one. However, 38% of sugar samples, with a low agreement, lie in classes four and  
 294 five, which are extended fish and flower type classes (Section 4.1). Note that even though  
 295 these samples reside in those regions of the feature space, their confidence is less than  
 296 25%. Similarly, in the gravel pattern, 21% samples belong to class six and exhibit min-  
 297 imal human confidence. In contrast, the rest from the gravel class are positioned between  
 298 classes one and seven, suggesting that gravel cloud cell sizes fall between sugar and flower.  
 299 Rightly, no human-labeled samples are found in class three, which predominantly com-  
 300 prise deep convective cells. Finally, the fish class exhibits relatively higher confidence in  
 301 human labels, aligning well with the feature space characteristics, and lies in class two  
 302 (fish) and four (extended fish-type cloud structures with large cloud-free regions). Hence,  
 303 cloud systems characterized by higher agreement among human observers are situated  
 304 within the designated regions, while those with lesser consensus are positioned within  
 305 the ambiguous regions of the continuum.

306 To compensate for the limited number of human label samples, we analyze the 30  
 307 nearest satellite images to each human label as identified by N1 (Fig. 2.c). This anal-  
 308 ysis aims to show the generalization capacity of our approach and further enhance our  
 309 understanding of the connection between organizations. The majority of neighbors in  
 310 human-identified fish-type cloud systems (more than 50%) belong to machine-identified  
 311 classes two and four. The gravel regime includes members of all classes, with notable con-  
 312 tributions from classes one, five, and seven, which exhibit cloud cell characteristics sim-  
 313 ilar to gravel systems. The variability in the spread can be linked to the limited repre-  
 314 sentation of gravel glass in Schulz (2022)’s dataset, as gravel occurrences were sporadic  
 315 during the EUREC<sup>4</sup>A campaign. Additionally, 75% of gravel labels in our sub-samples

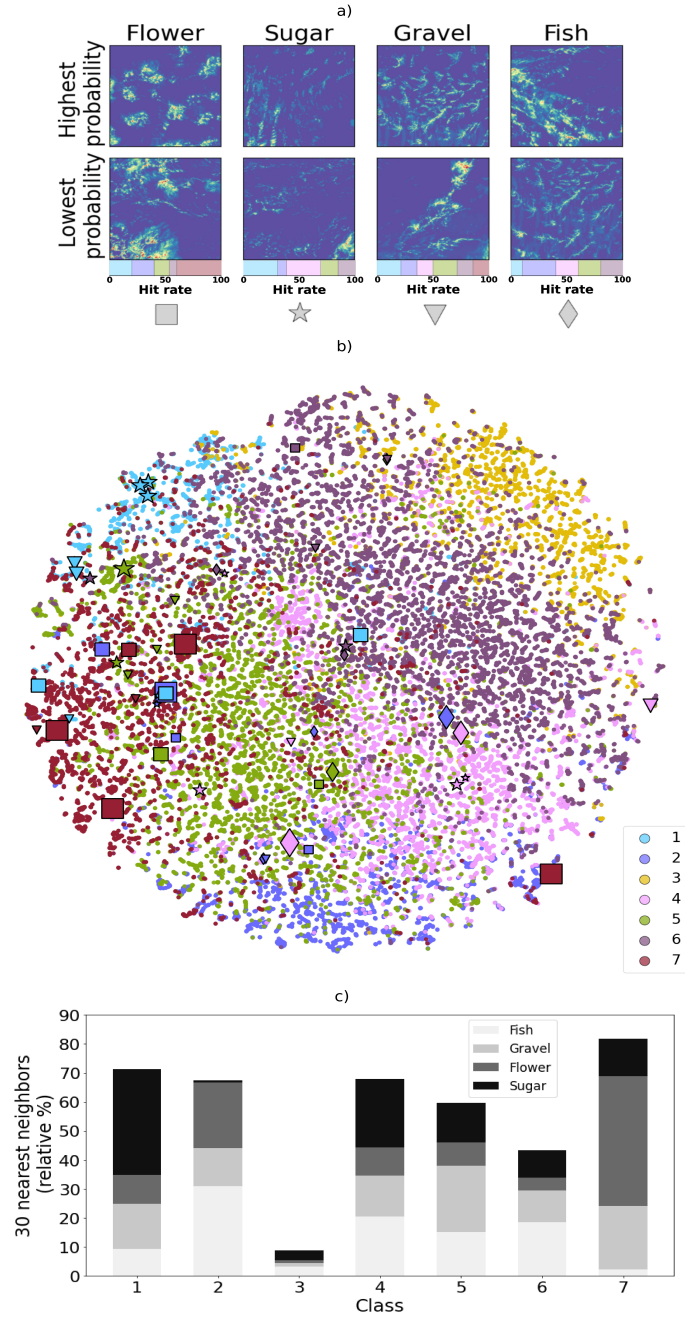


**Figure 2.** a) To enhance visualization and reference for human labels, each column displays 256 x 256 COD images of a specific class, with the highest and lowest human agreement shown in two rows. Below, the images in each column show the hit rate, representing the N2-predicted class for each human label. b) Continuum space colored with different classes (1-7) in the background, along with Human labels (fish, sugar, flower, gravel) in the foreground. Ascending symbol sizes with low (0-0.25), mid-low (0.25-0.50), mid-high (0.50-0.75), and high (0.75-1.00) agreement are shown. c) Relative occurrence of 30 nearest neighbors to human-labeled fish, gravel, flower, and sugar along the seven machine-labeled classes.

316 had agreement levels below 0.25. In contrast, the flower regime mainly belongs to class  
 317 seven (46 %), further aligning with the high confidence of human labels. Regarding sugar-  
 318 type cloud systems, 37 % of the neighbors fall into class one, while those with low hu-  
 319 man agreement are scattered across the remaining classes. Therefore, we find that machine-  
 320 labeled classes of the 30 nearest neighbors encompass the human-labeled ones, especially  
 321 for sugar, flower, and fish, but not so clearly for gravel.

322 Further, in S6, using ERA-5 large-scale environmental variables and cloud phys-  
 323 ical properties, we demonstrate that both the neighbors and the human crops share a  
 324 similar, homogeneous distribution of physical properties. Therefore, comparing human  
 325 labels with their nearest neighbors shows that the framework can understand the con-  
 326 nections between different cloud organizations, revealing the potential of representation  
 327 learning.

## 328 5 Transitions

329 To showcase an application that highlights the intelligible partitioning of the con-  
 330 tinuum, we explore the "sugar" to "flower" (S2F) cloud system transition on February  
 331 2, 2020. Using LES, Narenpitak et al. (2021) showed a strengthening of large-scale up-  
 332 ward wind motion and an increase in total water path and optical depth as the trans-  
 333 formation develops towards the flower. Here, we look at how the transition in COD is  
 334 represented in the feature space. For example, where do the representations of transi-  
 335 tions lie in the feature space? How smooth is the transition in the feature space?

336 Covering the temporal developments, 47 COD images were collected (after apply-  
 337 ing quality filter checks (see Section 2)), centered at 12.5° N, 50° W. They cover the time  
 338 from 10:50 to 19:20 UTC, with a gap between 17:00 to 18:00 UTC likely caused by lo-  
 339 cal sun glint. We ingested the available samples into the trained framework and collected  
 340 their features (from N1) and machine labels (from N2).

341 Sugar systems comprise small and shallow clouds with a large spread of individ-  
 342 ual cloud cells in a domain, as evident in the beginning (10:50, Fig. 3.a). In contrast,  
 343 flower systems appear in multiple deeper aggregates surrounded by large dry areas and  
 344 are detected first in the southeast cover at 16:50 before becoming dominated at 19:20  
 345 over the full domain. In general, the transition features lie at the border of well-defined  
 346 clusters one ('sugar') and cluster seven ('flower') (Fig. 3.a), and the framework is able  
 347 to capture their intermediary nature as they are neither perfect sugar nor flower type.  
 348 We use wind speed (vertical and horizontal) to represent changes in atmospheric dynam-  
 349 ics and changes in cloud cover to account for the changes in mesoscale structure from  
 350 the ERA-5 product. A gradual increase in vertical velocity is observed as the system tran-  
 351 sitions from S2F, and consequently, the surface wind speed gradually reduces its strength  
 352 (Fig. 3.b). In addition, as expected, cloud fraction profiles show a gradual decrease as  
 353 the transition progresses with time.

354 Sugar-type mesoscale organizations typically occur during the daytime with shal-  
 355 low boundary layers, while flowers occur at night with deeper boundary layers (Vial et  
 356 al., 2021). We use cosine distance between the features to show the gradual development  
 357 of the S2F transition inside the feature space (Fig. 3.c). The transformation appears smooth  
 358 initially, with relatively more significant changes occurring later (post-18:00 UTC) as the  
 359 system approaches the flower state. We link the relatively high changes in cosine distance  
 360 during flower stages, as opposed to initial sugar stages, to the progression of convective  
 361 developments. It becomes more accelerated as the system approaches the well-defined  
 362 flower state.

363 Therefore, the framework reveals unbiased relative changes from the point of in-  
 364 terest (in space or time) solely based on changes captured in high-dimensional feature  
 365 space. Also, the intelligible partitioning of the continuum allows us to see when a par-

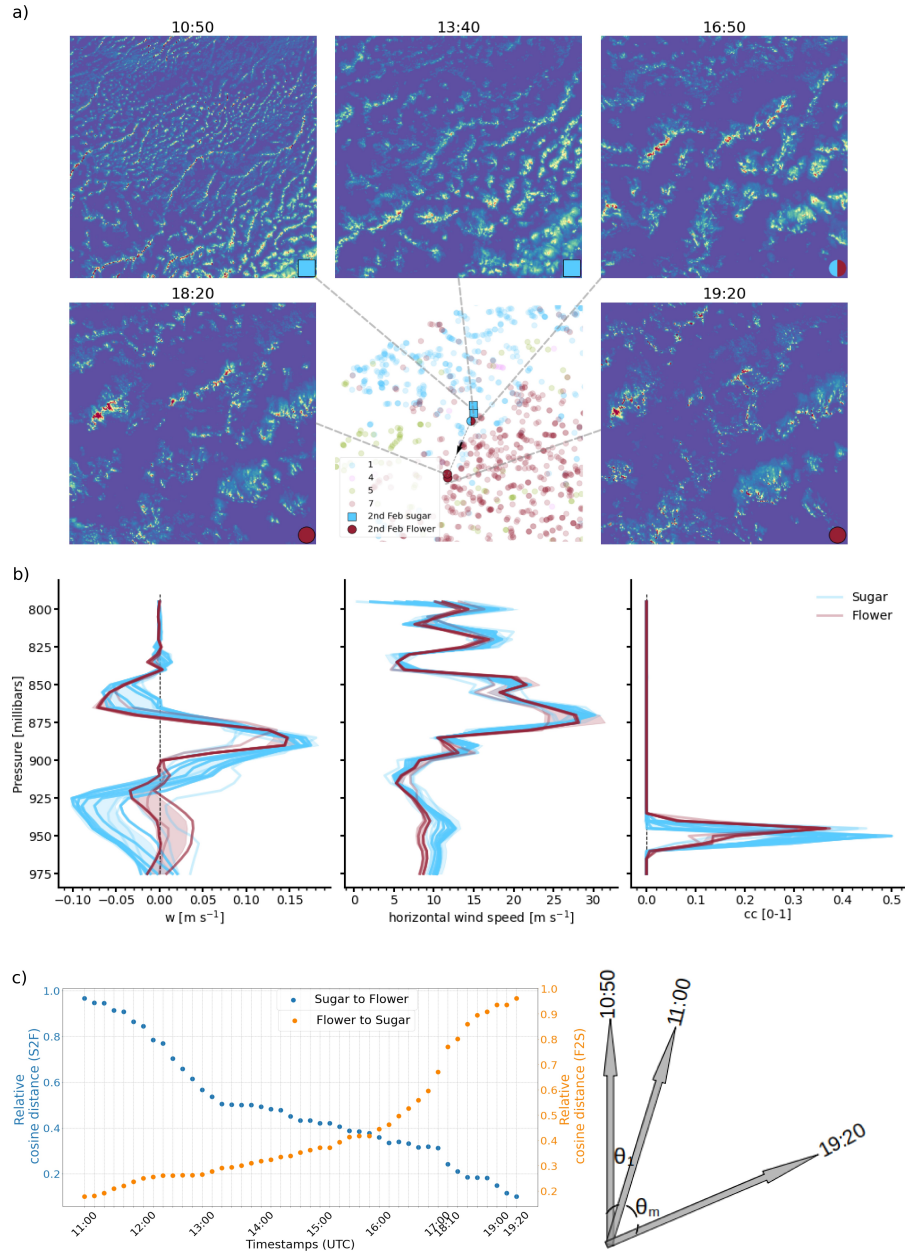


**Figure 3.** a) Five COD images covering the transition period between sugar and flower on the second of February 2020. Their position in the continuum is indicated in the center of the bottom row. b) Individual and standard deviation profiles of 1) vertical, 2) horizontal wind speed describing the atmospheric dynamics, and 3) cloud cover showing changes in mesoscale structure of the transition samples. c) Illustration of temporal transition development inside the feature space: cosine distance of the first daytime image feature obtained at 10:50 UTC compared with the cloud system evolution features for the rest of the day (blue). The last obtained image at 19:20 UTC towards the first image (orange) and  $\theta_m$  represents the increasing cosine distance.

366  
367

ticular system transitions to another. S7 provides insights into the transition probability of one class transforming to another over the Barbados domain.

## 6 Conclusion

In this work, we develop a two-step self-supervised learning framework to study shallow convective organization properties and their transitions. By analyzing organization in a continuous approach without imposing predefined classes, we include all occurring patterns and transitional states in our analysis. Moreover, the approach shows that mesoscale cloud organizations in NAT can be partitioned into seven optimal classes for the time period considered. Exploiting the cloud amount at different vertical levels from CERES measurements, we show how the classes are interlinked with each other within the continuous space and thus capture the variability of tropical clouds in more detail.

We compare human-labeled cloud systems (Schulz, 2022) in the machine-identified cluster regions. Cloud systems with higher agreement among humans lie in the "correct" region of the feature space, while the ones with less consensus are in the "wrong" regions of the feature space. Also, the potential and interpretability of the continuum space become more evident when examining the classification and physical properties between human labels and their nearest neighbors. Two of the seven optimal classes are strongly related to flower and sugar, respectively. Representing the S2F transition case study (Narenpitak et al., 2021) for February 2, 2020, in the continuum illustrates the capability to identify and represent the observed transformations smoothly in their clearly interpretable regions. We evaluate the transition's large-scale environmental parameters and observe a gradual increase in vertical wind speed and a gradual decrease in cloud amount. Finally, we demonstrate the framework's capability to capture the underlying mesoscale visual transformations, such as the transition approaching mature flower convective stages through quick changes in consecutive cosine distances.

One of the limitations of this study is that we use only the daytime cloud retrievals, and hence, the nocturnal nature of the organizations cannot be captured. Future studies will use infrared satellite measurements for 24-hour coverage. We aim to fine-tune our framework with the ground-based observations of the EUREC<sup>4</sup>A campaign and further extend our analysis to a climate scale. Currently, Destination Earth (Hoffmann et al., 2023) focuses on simulating high-resolution global digital twins at a 1 km grid scale. The developed workflow could be a testing ground for investigating the newly adjusted subgrid parameterization effects on mesoscale cloud systems or atmospheric processes at different scales.

## 7 Open Research

CERES, Edition-4A, DOI:10.5067/TERRA+AQUA/CERES/SYN1DEG-1HOUR.L3.004A) is made available by the NASA CERES group. ERA-5 reanalyses were downloaded from the Copernicus climate change services DOI:10.24381/cds.143582cf. GOES-16 COD data has been retrieved from Andy Walther, University of Wisconsin–Madison.

The code to produce this work and pre-trained weights of N1 and N2 can be accessed at <https://doi.org/10.5281/zenodo.8352614>

## Acknowledgments

Dwaipayan Chatterjee's research was supported by the Federal Ministry for Environment, Nature Conservation, Nuclear Safety, and Consumer Protection. Claudia Acquistapace's (CA) research was funded by Deutsche Forschungsgemeinschaft (DFG). CA also acknowledges funding from Federal Ministry for Digital and Transport (BMDV).

## References

Aggarwal, C. C., Hinneburg, A., & Keim, D. A. (2001). On the surprising behav-

- ior of distance metrics in high dimensional space. In J. Van den Bussche & V. Vianu (Eds.), *Database theory — icdt 2001* (pp. 420–434). Berlin, Heidelberg: Springer Berlin Heidelberg.
- Bebis, G., & Georgiopoulos, M. (1994). Feed-forward neural networks. *IEEE Potentials*, 13(4), 27–31. doi: 10.1109/45.329294
- Bony, S., Dufresne, J., Treut, H. L., Morcrette, J. J., & Senior, C. A. (2004). On dynamic and thermodynamic components of cloud changes. *Climate Dynamics*, 22, 71–86. Retrieved from <https://api.semanticscholar.org/CorpusID:56077074>
- Bony, S., & Dufresne, J.-L. (2005). Marine boundary layer clouds at the heart of tropical cloud feedback uncertainties in climate models. *Geophysical Research Letters*, 32(20). doi: 10.1029/2005GL023851
- Bony, S., Schulz, H., Vial, J., & Stevens, B. (2020). Sugar, Gravel, Fish, and Flowers: Dependence of Mesoscale Patterns of Trade-Wind Clouds on Environmental Conditions. *Geophysical Research Letters*, 47(7), e2019GL085988. doi: 10.1029/2019GL085988
- Bony, S., Stevens, B., Ament, F., Bigorre, S., Chazette, P., Crewell, S., ... Wirth, M. (2017, November). EUREC4A: A Field Campaign to Elucidate the Couplings Between Clouds, Convection and Circulation. *Surveys in Geophysics*, 38(6), 1529–1568. doi: 10.1007/s10712-017-9428-0
- Caliński, T., & Harabasz, J. (1974). A dendrite method for cluster analysis. *Communications in Statistics*, 3(1), 1–27. Retrieved from <https://www.tandfonline.com/doi/abs/10.1080/03610927408827101> doi: 10.1080/03610927408827101
- Caron, M., Touvron, H., Misra, I., Jégou, H., Mairal, J., Bojanowski, P., & Joulin, A. (2021). *Emerging properties in self-supervised vision transformers*.
- Chatterjee, D., Acquistapace, C., Deneke, H., & Crewell, S. (2023). Understanding cloud systems structure and organization using a machine’s self-learning approach. *Artificial Intelligence for the Earth Systems*. Retrieved from <https://journals.ametsoc.org/view/journals/aies/aop/AIES-D-22-0096.1/AIES-D-22-0096.1.xml> doi: <https://doi.org/10.1175/AIES-D-22-0096.1>
- Dauhut, T., Couvreur, F., Bouniol, D., Beucher, F., Volkmer, L., Pörtge, V., ... Wirth, M. (2023). Flower trade-wind clouds are shallow mesoscale convective systems. *Quarterly Journal of the Royal Meteorological Society*, 149(750), 325–347. doi: 10.1002/qj.4409
- Denby, L. (2020). Discovering the Importance of Mesoscale Cloud Organization Through Unsupervised Classification. *Geophysical Research Letters*, 47(1), e2019GL085190. doi: 10.1029/2019GL085190
- Denby, L. (2023). *Charting the realms of mesoscale cloud organisation using unsupervised learning*. doi: 10.48550/arXiv.2309.08567
- Du, X. (2023). A robust and high-dimensional clustering algorithm based on feature weight and entropy. *Entropy*, 25(3). Retrieved from <https://www.mdpi.com/1099-4300/25/3/510> doi: 10.3390/e25030510
- Gilpin, S., Qian, B., & Davidson, I. (2013). Efficient hierarchical clustering of large high dimensional datasets. In *Proceedings of the 22nd acm international conference on information & knowledge management* (p. 1371–1380). New York, NY, USA: Association for Computing Machinery. Retrieved from <https://doi.org/10.1145/2505515.2505527> doi: 10.1145/2505515.2505527
- Goyal, P., Duval, Q., Reizenstein, J., Leavitt, M., Xu, M., Lefaudeux, B., ... Misra, I. (2021). *Vissl*. <https://github.com/facebookresearch/vissl>.
- Hersbach, H., Bell, B., Berrisford, P., Hirahara, S., Horányi, A., Muñoz-Sabater, J., ... Thépaut, J.-N. (2020). The era5 global reanalysis. *Quarterly Journal of the Royal Meteorological Society*, 146(730), 1999–2049. doi: <https://doi.org/10.1002/qj.3803>
- Hoffmann, J., Bauer, P., Sandu, I., Wedi, N., Geenen, T., & Thiemert, D. (2023).

- 469 Destination earth – a digital twin in support of climate services. *Climate*  
 470 *Services*, 30, 100394. Retrieved from [https://www.sciencedirect.com/](https://www.sciencedirect.com/science/article/pii/S2405880723000559)  
 471 [science/article/pii/S2405880723000559](https://www.sciencedirect.com/science/article/pii/S2405880723000559) doi: [https://doi.org/10.1016/](https://doi.org/10.1016/j.cliser.2023.100394)  
 472 [j.cliser.2023.100394](https://doi.org/10.1016/j.cliser.2023.100394)
- 473 Huynh, T., Kornblith, S., Walter, M. R., Maire, M., & Khademi, M. (2022). *Boost-*  
 474 *ing contrastive self-supervised learning with false negative cancellation.*
- 475 Janssens, M., Vilà-Guerau de Arellano, J., Scheffer, M., Antonissen, C., Siebesma,  
 476 A. P., & Glassmeier, F. (2021). Cloud Patterns in the Trades Have Four In-  
 477 terpretable Dimensions. *Geophysical Research Letters*, 48(5), e2020GL091001.  
 478 doi: 10.1029/2020GL091001
- 479 Khan, S., Naseer, M., Hayat, M., Zamir, S. W., Khan, F. S., & Shah, M. (2022,  
 480 jan). Transformers in vision: A survey. *ACM Computing Surveys*, 54(10s),  
 481 1–41. doi: 10.1145/3505244
- 482 Muller, C. J., & Held, I. M. (2012, August). Detailed Investigation of the Self-  
 483 Aggregation of Convection in Cloud-Resolving Simulations. *Journal of the At-*  
 484 *mospheric Sciences*, 69(8), 2551–2565. (Publisher: American Meteorological  
 485 Society Section: Journal of the Atmospheric Sciences) doi: 10.1175/JAS-D-11-  
 486 -0257.1
- 487 Narenpitak, P., Kazil, J., Yamaguchi, T., Quinn, P., & Feingold, G. (2021). From  
 488 Sugar to Flowers: A Transition of Shallow Cumulus Organization Dur-  
 489 ing ATOMIC. *Journal of Advances in Modeling Earth Systems*, 13(10),  
 490 e2021MS002619. doi: 10.1029/2021MS002619
- 491 Nie, Y., Zamzam, A. S., & Brandt, A. (2021). Resampling and data augmenta-  
 492 tion for short-term pv output prediction based on an imbalanced sky images  
 493 dataset using convolutional neural networks. *Solar Energy*, 224, 341-354.  
 494 Retrieved from [https://www.sciencedirect.com/science/article/pii/](https://www.sciencedirect.com/science/article/pii/S0038092X21004795)  
 495 [S0038092X21004795](https://www.sciencedirect.com/science/article/pii/S0038092X21004795) doi: <https://doi.org/10.1016/j.solener.2021.05.095>
- 496 Nuijens, L., & Siebesma, A. P. (2019, June). Boundary Layer Clouds and Convec-  
 497 tion over Subtropical Oceans in our Current and in a Warmer Climate. *Cur-*  
 498 *rent Climate Change Reports*, 5(2), 80–94. doi: 10.1007/s40641-019-00126-x
- 499 Paletta, Q., Terrén-Serrano, G., Nie, Y., Li, B., Bieker, J., Zhang, W., ... Feng,  
 500 C. (2023). Advances in solar forecasting: Computer vision with deep learn-  
 501 ing. *Advances in Applied Energy*, 11, 100150. Retrieved from [https://](https://www.sciencedirect.com/science/article/pii/S266679242300029X)  
 502 [www.sciencedirect.com/science/article/pii/S266679242300029X](https://www.sciencedirect.com/science/article/pii/S266679242300029X) doi:  
 503 <https://doi.org/10.1016/j.adapen.2023.100150>
- 504 Paszke, A., Gross, S., Massa, F., Lerer, A., Bradbury, J., Chanan, G., ... Chin-  
 505 tala, S. (2019). *Pytorch: An imperative style, high-performance deep learning*  
 506 *library.*
- 507 Rousseeuw, P. J. (1987). Silhouettes: A graphical aid to the interpretation and val-  
 508 idation of cluster analysis. *Journal of Computational and Applied Mathemat-*  
 509 *ics*, 20, 53-65. Retrieved from [https://www.sciencedirect.com/science/](https://www.sciencedirect.com/science/article/pii/0377042787901257)  
 510 [article/pii/0377042787901257](https://www.sciencedirect.com/science/article/pii/0377042787901257) doi: [https://doi.org/10.1016/0377-0427\(87\)](https://doi.org/10.1016/0377-0427(87)90125-7)  
 511 [90125-7](https://doi.org/10.1016/0377-0427(87)90125-7)
- 512 Sarkar, M., Zuidema, P., Albrecht, B., Ghate, V., Jensen, J., Mohrmann, J., &  
 513 Wood, R. (2020). Observations pertaining to precipitation within the north-  
 514 east pacific stratocumulus-to-cumulus transition. *Monthly Weather Review*,  
 515 148(3), 1251 - 1273. doi: 10.1175/MWR-D-19-0235.1
- 516 Schmit, T. J., Gunshor, M. M., Menzel, W. P., Gurka, J. J., Li, J., & Bachmeier,  
 517 A. S. (2005). Introducing the next-generation advanced baseline imager on  
 518 goes-r. *Bulletin of the American Meteorological Society*, 86(8), 1079 - 1096.  
 519 Retrieved from [https://journals.ametsoc.org/view/journals/bams/86/8/](https://journals.ametsoc.org/view/journals/bams/86/8/bams-86-8-1079.xml)  
 520 [bams-86-8-1079.xml](https://journals.ametsoc.org/view/journals/bams/86/8/bams-86-8-1079.xml) doi: <https://doi.org/10.1175/BAMS-86-8-1079>
- 521 Schneider, T., Kaul, C., & Pressel, K. (2019, 03). Possible climate transitions  
 522 from breakup of stratocumulus decks under greenhouse warming. *Nature*  
 523 *Geoscience*, 12, 164-168. doi: 10.1038/s41561-019-0310-1

- 524 Schubert, E. (2023, jun). Stop using the elbow criterion for k-means and how to  
 525 choose the number of clusters instead. *ACM SIGKDD Explorations Newsletter*,  
 526 25(1), 36–42. doi: 10.1145/3606274.3606278
- 527 Schulz, H. (2022). C<sup>3</sup>ontext: a common consensus on convective organization during  
 528 the eurec<sup>4</sup>a experiment. *Earth System Science Data*, 14(3), 1233–1256. doi: 10  
 529 .5194/essd-14-1233-2022
- 530 Schulz, H., Eastman, R., & Stevens, B. (2021). Characterization and Evolution  
 531 of Organized Shallow Convection in the Downstream North Atlantic Trades.  
 532 *Journal of Geophysical Research: Atmospheres*, 126(17), e2021JD034575. doi:  
 533 10.1029/2021JD034575
- 534 Steinbach, M., Ertöz, L., & Kumar, V. (2004). The challenges of clustering high  
 535 dimensional data. In L. T. Wille (Ed.), *New directions in statistical physics:  
 536 Econophysics, bioinformatics, and pattern recognition* (pp. 273–309). Berlin,  
 537 Heidelberg: Springer Berlin Heidelberg. Retrieved from [https://doi.org/  
 538 10.1007/978-3-662-08968-2\\_16](https://doi.org/10.1007/978-3-662-08968-2_16) doi: 10.1007/978-3-662-08968-2\_16
- 539 Stevens, B., Bony, S., Brogniez, H., Hentgen, L., Hohenegger, C., Kiemle, C., ...  
 540 Zuidema, P. (2020). Sugar, gravel, fish and flowers: Mesoscale cloud patterns  
 541 in the trade winds. *Quarterly Journal of the Royal Meteorological Society*,  
 542 146(726), 141–152. doi: 10.1002/qj.3662
- 543 Stevens, B., Bony, S., Farrell, D., Ament, F., Blyth, A., Fairall, C., ... Zöger, M.  
 544 (2021, August). EUREC<sup>4</sup>A. *Earth System Science Data*, 13(8), 4067–4119.  
 545 (Publisher: Copernicus GmbH) doi: 10.5194/essd-13-4067-2021
- 546 Stevens, B., Farrell, D., Hirsch, L., Jansen, F., Nuijens, L., Serikov, I., ... Prospero,  
 547 J. M. (2016). The barbados cloud observatory: Anchoring investigations  
 548 of clouds and circulation on the edge of the itcz. *Bulletin of the Ameri-  
 549 can Meteorological Society*, 97(5), 787 - 801. doi: [https://doi.org/10.1175/  
 550 BAMS-D-14-00247.1](https://doi.org/10.1175/<br/>
  550 BAMS-D-14-00247.1)
- 551 van der Maaten, L., & Hinton, G. (2008). Visualizing data using t-sne. *Journal  
 552 of Machine Learning Research*, 9(86), 2579–2605. Retrieved from [http://jmlr  
 553 .org/papers/v9/vandermaaten08a.html](http://jmlr<br/>
  553 .org/papers/v9/vandermaaten08a.html)
- 554 Vaswani, A., Shazeer, N., Parmar, N., Uszkoreit, J., Jones, L., Gomez, A. N.,  
 555 ... Polosukhin, I. (2023). *Attention is all you need*. Retrieved from  
 556 <https://arxiv.org/abs/1706.03762>
- 557 Vial, J., Vogel, R., & Schulz, H. (2021). On the daily cycle of mesoscale cloud organ-  
 558 ization in the winter trades. *Quarterly Journal of the Royal Meteorological So-  
 559 ciety*, 147(738), 2850–2873. doi: 10.1002/qj.4103
- 560 Vogel, R., Konow, H., Schulz, H., & Zuidema, P. (2021, November). A climatology  
 561 of trade-wind cumulus cold pools and their link to mesoscale cloud organiza-  
 562 tion. *Atmospheric Chemistry and Physics*, 21(21), 16609–16630. (Publisher:  
 563 Copernicus GmbH) doi: 10.5194/acp-21-16609-2021
- 564 Walther, A., & Heidinger, A. K. (2012). Implementation of the daytime cloud op-  
 565 tical and microphysical properties algorithm (dcomp) in patmos-x. *Journal of  
 566 Applied Meteorology and Climatology*, 51(7), 1371 - 1390. doi: 10.1175/JAMC  
 567 -D-11-0108.1
- 568 Wielicki, B., Barkstrom, B., Harrison, E., Lee, R., Smith, G., & Cooper, J. (1996,  
 569 05). Clouds and the earth’s radiant energy system (ceres): An earth observing  
 570 system experiment. *Bulletin of the American Meteorological Society*, 77, 853-  
 571 868. doi: 10.1175/1520-0477(1996)077<0853:CATERE>2.0.CO;2

## 572 References From the Supporting Information

- 573 Aggarwal, C. C., Hinneburg, A., Keim, D. A. (2001). On the surprising behavior  
 574 of distance metrics in high dimensional space. In J. Van den Bussche V. Vianu (Eds.),  
 575 Database theory — icdt 2001 (pp. 420–434). Berlin, Heidelberg: Springer Berlin Hei-  
 576 delberg.

- 577 Bottou, L. (2012). Stochastic gradient descent tricks. In G. Montavon, G. B. Orr,  
578 K.R. Müller (Eds.), *Neural networks: Tricks of the trade: Second edition* (pp. 421–436).  
579 Berlin, Heidelberg: Springer Berlin Heidelberg. doi: 10.1007/978-3-642-35289-8\_25
- 580 Bridle, J. S. (1989). Probabilistic interpretation of feedforward classification net-  
581 work outputs, with relationships to statistical pattern recognition. In *Nato neurocom-*  
582 *puting*. Retrieved from <https://api.semanticscholar.org/CorpusID:59636530>
- 583 Caron, M., Touvron, H., Misra, I., Jégou, H., Mairal, J., Bojanowski, P., Joulin,  
584 A. (2021). Emerging properties in self-supervised vision transformers.
- 585 Dosovitskiy, A., Beyer, L., Kolesnikov, A., Weissenborn, D., Zhai, X., Unterthiner,  
586 T., Houlsby, N. (2021). An image is worth 16x16 words: Transformers for image recog-  
587 nition at scale.
- 588 Fukushima, K. (1975). Cognitron: A self-organizing multilayered neural network.  
589 *Biological Cybernetics*, 20 (3-4), 121–136. Retrieved 2022-08-30, from [http://link.springer](http://link.springer.com/10.1007/BF00342633)  
590 [.com/10.1007/BF00342633](http://link.springer.com/10.1007/BF00342633)doi:10.1007/BF00342633
- 591 He, K., Zhang, X., Ren, S., Sun, J. (2015, December). Deep Residual Learning for  
592 Image Recognition. Retrieved 2022-08-30, from <http://arxiv.org/abs/1512.03385> (arXiv:1512.03385  
593 [cs])
- 594 Hendrycks, D., Gimpel, K. (2023). Gaussian error linear units (gelus). Retrieved  
595 from <https://arxiv.org/abs/1606.08415>
- 596 Khan, S., Naseer, M., Hayat, M., Zamir, S. W., Khan, F. S., Shah, M. (2022, jan).  
597 Transformers in vision: A survey. *ACM Computing Surveys*, 54 (10s), 1–41. doi: 10.1145/3505244
- 598 Rumelhart, D. E., Hinton, G. E., Williams, R. J. (1986, October). Learning rep-  
599 resentations by back-propagating errors. *Nature*, 323 (6088), 533–536. Retrieved from  
600 <https://doi.org/10.1038/323533a0> doi: 10.1038/323533a0
- 601 Tenenbaum, J. B., de Silva, V., Langford, J. C. (2000). A global geometric frame-  
602 work for nonlinear dimensionality reduction. *Science*, 290 (5500), 2319–2323. Retrieved  
603 from <https://www.science.org/doi/abs/10.1126/science.290.5500.2319> doi: 10.1126/sci-  
604 ence.290.5500.2319
- 605 Vaswani, A., Shazeer, N., Parmar, N., Uszkoreit, J., Jones, L., Gomez, A. N., . .  
606 . Polosukhin, I. (2023). Attention is all you need. Retrieved from [https://arxiv.org/](https://arxiv.org/abs/1706.03762)  
607 [abs/1706.03762](https://arxiv.org/abs/1706.03762)